

PAct: Part-Decomposed Single-View Articulated Object Generation

QINGMING LIU, The Chinese University of Hong Kong, Shenzhen, China and DexForce Technology, China

XINYUE YAO, The Chinese University of Hong Kong, Shenzhen, China

SHUYUAN ZHANG, The Chinese University of Hong Kong, Shenzhen, China

YUECI DENG, The Chinese University of Hong Kong, Shenzhen, China and DexForce Technology, China

GUILIANG LIU, The Chinese University of Hong Kong, Shenzhen, China

ZHEN LIU*, The Chinese University of Hong Kong, Shenzhen, China

KUI JIA, The Chinese University of Hong Kong, Shenzhen, China and DexForce Technology, China



Fig. 1. Given a single image, **PAct** generates an articulated 3D object by predicting a part-decomposed structure, synthesizing high-fidelity part geometry and appearance, and estimating articulation parameters for physics-based simulation.

Articulated objects are central to interactive 3D applications, including embodied AI, robotics, and VR/AR, where functional part decomposition and kinematic motion are essential. Yet producing high-fidelity articulated assets remains difficult to scale because it requires reliable part decomposition and kinematic rigging. Existing approaches largely fall into two paradigms: optimization-based reconstruction or distillation, which can be accurate but often takes tens of minutes to hours per instance, and inference-time

*Corresponding author.

Authors' Contact Information: Qingming Liu, qingmingliu@foxmail.com, The Chinese University of Hong Kong, Shenzhen, China and DexForce Technology, China; Xinyue Yao, xinyueyao1@link.cuhk.edu.cn, The Chinese University of Hong Kong, Shenzhen, China; Shuyuan Zhang, The Chinese University of Hong Kong, Shenzhen, China, rayzhang707@gmail.com; Yueci Deng, yuecideng@link.cuhk.edu.cn, The Chinese University of Hong Kong, Shenzhen, China and DexForce Technology, China; Guiliang Liu, The Chinese University of Hong Kong, Shenzhen, China, guiliangliu@cuhk.edu.cn; Zhen Liu, The Chinese University of Hong Kong, Shenzhen, China, zhenliu@cuhk.edu.cn; Kui Jia, The Chinese University of Hong Kong, Shenzhen, China and DexForce Technology, China, kuijia@cuhk.edu.cn.

methods that rely on template or part retrieval, producing plausible results that may not match the specific structure and appearance in the input observation. We introduce a part-centric generative framework for articulated object creation that synthesizes part geometry, composition, and articulation under explicit part-aware conditioning. Our representation models an object as a set of movable parts, each encoded by latent tokens augmented with part identity and articulation cues. Conditioned on a single image, the model generates articulated 3D assets that preserve instance-level correspondence while maintaining valid part structure and motion. The resulting approach avoids per-instance optimization, enables fast feed-forward inference, and supports controllable assembly and articulation, which are important for embodied interaction. Experiments on common articulated categories (e.g., drawers and doors) show improved input consistency, part accuracy, and articulation plausibility over optimization-based and retrieval-driven baselines, while substantially reducing inference time. Project page: <https://PAct-project.github.io>

Additional Key Words and Phrases: Generative models, Articulated objects, Embodied AI, 3D asset generation

1 Introduction

Articulated objects are pervasive in everyday environments. To faithfully replicate our interactive and physical world for applications such as virtual reality and simulators for embodied AI, it is important to reconstruct these objects and their articulation information from visual observations, ideally from single-view images. Despite recent progress in 3D reconstruction and generative 3D modeling, recovering object-specific articulation parameters and 3D representations from visual inputs remains challenging. In practice, results often require extensive manual cleanup, or even modeling from scratch before they are usable in production settings.

Existing efforts to create articulated objects from visual observations can be roughly categorized into two lines of work: optimization-based methods and optimization-free feedforward methods. The former reconstruct an articulated 3D asset by iteratively fitting geometry and articulation parameters with explicit visual supervision (images or videos) [Hsu et al. 2023; Jiang et al. 2022; Liu et al. 2023, 2025a,b], and/or by leveraging signals from pretrained generative models via techniques such as score distillation sampling [Chen et al. 2025a; Qiu et al. 2025]. Although these approaches can be highly accurate when rich, well-suited multi-view supervision is available, they are costly, often taking minutes to reconstruct a single instance, and can be prone to optimization failures since the underlying problem is inherently ill-posed. In the single-view setting, the constraints are much weaker, so the method leans more on the generative prior and optimization becomes less reliable. In contrast, recent feedforward reconstruction methods train networks that take visual inputs and directly output reconstructed 3D assets [Hong et al. 2023; Szymanowicz et al. 2024; Tang et al. 2024; Team 2024; Wang et al. 2024; Xiang et al. 2025, 2024]. These approaches have also been extended to reconstruct simulation-ready articulated objects, where both part structures (e.g., bounding boxes) and articulation relations are inferred [Liu et al. 2024a; Wu et al. 2025; Yuan et al. 2025]. However, existing methods often rely on template-based retrieval, which rarely yields accurate reconstructions, or train reconstruction models from scratch, which tends to generalize poorly given limited training data.

Motivated by these challenges, we propose **PAct**, a feedforward, part-decomposed generative framework for articulated object creation from a single image. We model an object as a set of movable parts, each with 3D geometry and appearance, together with articulation attributes (e.g., semantic label, joint type, axis, pivot, and motion range). For generalizable and faithful reconstruction, **PAct** is built by finetuning TRELLIS [Xiang et al. 2024], a pretrained two-stage 3D-native generative model, to directly generate part-decomposed 3D assets and their articulation parameters. Concretely, each object is encoded as a set of part latents, and the denoising transformer augments global attention with within-part attention to refine individual parts while preserving cross-part consistency. Along the diffusion sampling trajectory, we extract intermediate features from the denoising transformer at several timesteps, average them per part, and feed the resulting part features into a lightweight MLP to predict articulation parameters. This unified

design enables fast feedforward inference, remains faithful to the observed instance, and supports controllable part decomposition, assembly, and articulation in a single forward generation pipeline.

2 Related Works

Articulated Object Reconstruction. Articulated object reconstruction aims to recover both part geometry/appearance and kinematics from sparse observations. Early efforts leverage interaction or multi-state observations to build digital twins and estimate joint parameters, e.g., Ditto learns part-level geometry and articulation from before/after interaction pairs [Hsu et al. 2023; Jiang et al. 2022], while SfA [Nie et al. 2022] explores interaction-driven structure discovery for unseen objects [Nie et al. 2022]. Recent works increasingly exploit neural implicit fields and differentiable rendering to jointly optimize shape and motion: PARIS reconstructs part-level implicit fields and motion parameters in a self-supervised manner from multi-view observations of different states [Liu et al. 2023], and RE-ACTO [Song et al. 2024] extends reconstruction to casually captured monocular videos with quasi-rigid deformation to better preserve piecewise rigidity. Alongside method advances, large-scale real data and benchmarks facilitate evaluation in the wild, such as MultiScan for RGBD scanning and annotation of articulated objects in indoor scenes [Mao et al. 2022]. More recently, 3D Gaussian Splatting has become a strong representation for photorealistic articulated replicas: ArtGS and VideoArtGs align information across object states [Liu et al. 2025a,b], and SplArt [Lin et al. 2025a] further estimates kinematics and part-level reconstruction with self-supervised 3DGS [Kerbl et al. 2023] training from multi-state images. Finally, a growing line of work targets *feed-forward* articulated reconstruction for efficiency and scalability, e.g., Real2Code predicts URDF-style articulation via code generation from visual cues [Mandi et al. 2024], and recent large articulation reconstruction models push toward category-agnostic, multi-part settings [Li et al. 2025; Yuan et al. 2025].

Articulated Object Generation. Beyond reconstructing an observed instance, articulated object generation synthesizes novel assets with plausible part structures and motions. Graph-/structure informed generators explicitly model part connectivity and kinematics [He et al. 2025; Lei et al. 2023; Liu et al. 2024a,b; Wu et al. 2025]. MeshArt [Gao et al. 2024] proposed an auto-regressive method to model the geometry and articulation information. Another trend is *open-world* articulation via foundation models [Wang et al. 2025]: Articulate-Anything uses vision-language reasoning to segment parts and propose functional joints from diverse input modalities [Le et al. 2025], and open-vocabulary mesh-to-articulation frameworks further reduce category constraints by converting generic rigid meshes into articulated counterparts [Qiu et al. 2025]. Complementarily, training-free or hybrid paradigms reuse strong static 3D generators as priors, optimizing geometry/texture and joint parameters from a few articulated observations to avoid training on scarce articulated data [Chen et al. 2025a]. At the data/system level, scalable synthesis pipelines (e.g., procedural generation) are also emerging to provide high-fidelity articulated assets for downstream learning and generation [Lian et al. 2025].

3D Generative Model. Recent 3D generative models span fast feed-forward single-image reconstruction and scalable 3D foundation

modeling. TripoSR [Tochilkin et al. 2024] enables sub-second image-to-3D mesh reconstruction as a strong practical prior. TRELLIS unifies multi-format 3D decoding via a structured latent representation and improves fidelity with scalable conditional generation [Xiang et al. 2025, 2024]. Beyond holistic assets, part-based methods explicitly model compositional structure for controllability, including PartCrafter, PartPacker, OmniPart, and part-by-part pipelines such as PartGen and AutoPartGen [Chen et al. 2024, 2025b; Lin et al. 2025b; Tang et al. 2025; Yang et al. 2025]; \mathcal{X} -Part and P³-SAM provide strong 3D part decomposition/segmentation support [Ma et al. 2025; Yan et al. 2025]. Industrial systems (Hunyuan3D 2.0/2.5, Seed3D) further push high-fidelity, PBR- and simulation-ready asset generation [Seed3D Team 2025; Team 2025a,b].

3 Preliminary: TRELLIS – A 3D-Native Generative Model

Pretrained object-level 3D generative models provide strong priors for synthesizing high-quality geometry and appearance from limited observations. Given the scarcity of large-scale datasets for articulated objects, leveraging such pretrained 3D priors forms an effective foundation for our approach. In particular, **PAct** builds upon TRELLIS [Xiang et al. 2024], a two-stage 3D-native generative framework for producing detailed 3D representations of static objects from a single image or a text prompt.

Stage 1: Sparse Structure Generation. TRELLIS adopts a two-stage pipeline that generates 3D objects from coarse structure to fine-grained details. In the first stage, object geometry is represented as a sparse binary occupancy grid at a resolution of 64^3 . A variational autoencoder (VAE) encodes this sparse structure into a compact spatial latent representation:

$$z = E_{ss}(x) \in \mathbb{R}^{16 \times 16 \times 16 \times c}, \quad \hat{x} = D_{ss}(z), \quad (1)$$

where $x \in \mathbb{R}^{64 \times 64 \times 64}$ denotes the input occupancy grid, E_{ss} and D_{ss} are the encoder and decoder, and z is the resulting latent tensor. A rectified flow model \mathcal{RF}_{ss} is trained in this latent space to enable conditional generation of coarse object structures.

Stage 2: Geometry and Appearance Generation. To model fine-grained geometry and appearance, TRELLIS constructs a structured latent feature volume (SLAT):

$$\mathcal{F} = \{(x_i, f_i)\}_{i=1}^L, \quad x_i \in \{0, \dots, 63\}^3, \quad f_i \in \mathbb{R}^d, \quad (2)$$

where each occupied voxel location x_i is associated with a feature vector f_i extracted from image-based features. This sparse representation encodes detailed appearance information only at occupied locations.

The sparse feature volume is further encoded into a latent representation using a sparse encoder-decoder architecture:

$$\mathcal{Z} = E_{SLAT}(\mathcal{F}) = \{(x_i, z_i)\}_{i=1}^L, \quad \hat{\mathcal{Z}} = D_{SLAT}(\mathcal{Z}), \quad (3)$$

where $z_i \in \mathbb{R}^d$ denotes the latent feature at location x_i . A second rectified flow model, \mathcal{RF}_{SLAT} , is trained in this sparse latent space to enable conditional generation of detailed geometry and appearance, after which the decoder reconstructs the final 3D representation.

4 Method

4.1 Problem Definition

Given a single RGB image I as conditioning input, our goal is to reconstruct a complete articulated object representation O that is (i) geometrically consistent, (ii) visually faithful to the input image, and (iii) physically plausible with respect to its articulation structure. We assume the objects of interest admit a tree-structured articulation with a single root, which captures many articulated objects in practice.

Formally, we represent an articulated object as $O = \{\mathcal{P}_i\}_{i=1}^K$, $\mathcal{P}_i = (\mathcal{G}_i, \mathcal{A}_i)$, where K denotes the number of movable parts and each part \mathcal{P}_i is associated with both its 3D representation and articulation parameters. Specifically, each part \mathcal{P}_i is defined as where \mathcal{G}_i denotes the geometry and appearance of the i -th part, and \mathcal{A}_i encodes its articulation information.

We consider three joint types between a part and its parent in the articulation tree: *revolute* (hinge), *prismatic*, and *fixed*. Following prior work [Liu et al. 2024a,b], we parameterize the articulation of each part i using a compact set of joint parameters:

$$\mathcal{A}_i = \{\tau_i, s_i, o_i, u_i, \rho_i, q_i\}, \quad (4)$$

where τ_i denotes the joint type (e.g., *fixed*, *prismatic*, or *revolute*), s_i is a semantic label (e.g., base, door, drawer), $o_i \in \mathbb{R}^3$ is the joint origin (pivot point) in the world coordinate system, $u_i \in \mathbb{R}^3$ is the joint axis direction, $\rho_i = [\rho_i^{\min}, \rho_i^{\max}] \in \mathbb{R}^2$ specifies the valid motion range (e.g., lower/upper rotation limits in radians), and q_i indicates the parent of part i in the articulation tree. For numerical stability, we normalize the axis direction as $u_i \leftarrow u_i / \|u_i\|_2$.

4.2 Stage 1: Part-Decomposed Structure Generation

We represent the sparse structure of an articulated object using a set of part-level latent codes $Z_{\text{global}} = \{z_i\}_{i=1}^K$, where each latent vector z_i corresponds to part i and encodes its geometric attributes, and K denotes the number of parts in the object. To distinguish different parts, we introduce learnable part-identity embeddings $E \in \mathbb{R}^{T \times d_p}$, where T is a preset maximum number of parts and each row $E[t]$ provides an identity embedding for the t -th part index. We then form the final latent representation for each part by concatenating the part latent code with its identity embedding: $z_i = [z_i \parallel E[i]]$.

Part-aware Denoising Transformer. As TRELLIS is pretrained to model a single coherent object, during fine-tuning we repurpose a subset of attention layers to operate within each part (details in the sec. 5.1), so that the model can reuse its pretrained object-level modeling at the part level, while the remaining layers retain global attention to capture interactions between parts.

Within-part Local Attention. In the repurposed layers, self-attention is restricted to tokens belonging to the same part. For part i , the within-part self-attention is defined as

$$H_i = z_i + \text{Attn}(z_i W_Q^p, z_i W_K^p, z_i W_V^p), \quad (5)$$

where $\text{Attn}(Q, K, V) = \text{Softmax}\left(\frac{QK^T}{\sqrt{d}}\right)V$. As in standard attention layers, this is followed by a feedforward network (FFN) with a residual connection $H_i \leftarrow H_i + \text{FFN}(H_i)$.

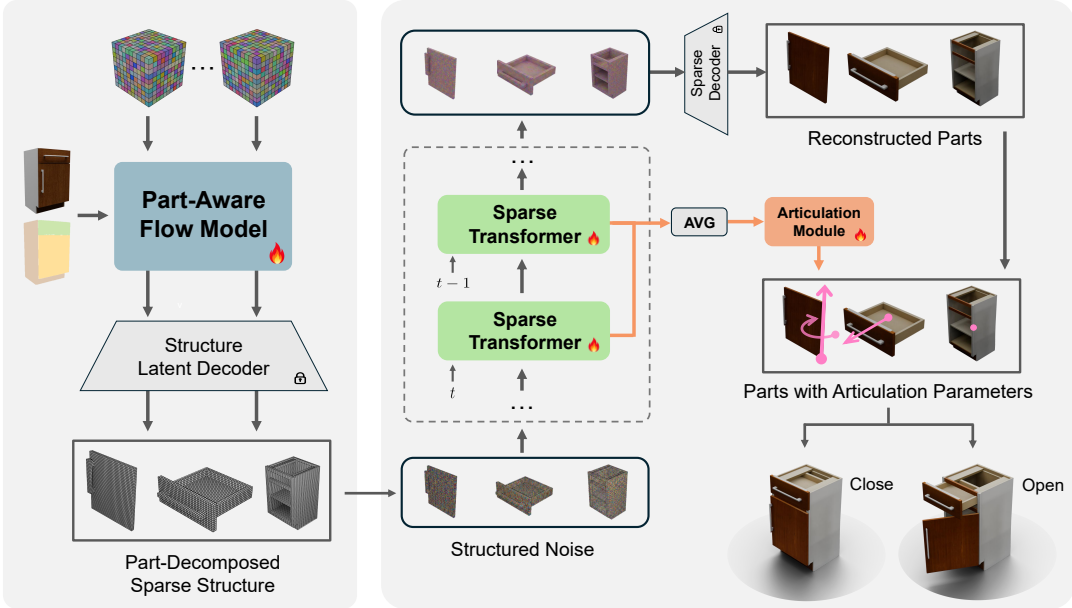


Fig. 2. Pipeline of **PAct**. Stage 1 predicts a part-decomposed sparse structure from a single image using a Part-Aware Flow Model. Stage 2 refines it into detailed 3D part representations via sparse-transformer denoising, while an articulation module aggregates multi-step features to estimate joint parameters for each part. The predicted joint parameters together with the reconstructed part geometries form the final articulated object.

Mask-based Part Conditioning. To provide explicit spatial guidance for part decomposition, we additionally condition the model on a 2D part mask \mathcal{M} . The mask assigns a discrete part index to each image location, and we embed it using the same part identity embedding \mathbf{E} to ensure consistent part semantics between image-space conditioning and part-level latents. Given a mask $\mathcal{M} \in \{0, 1, \dots, T-1\}^{h \times w}$, we construct a dense part-embedding map

$$\mathbf{P}_{u,v} = \mathbf{E}[\mathcal{M}_{u,v}] \in \mathbb{R}^{dp}, \quad (6)$$

which is subsequently downsampled and added to the image features extracted by DINOv2 [Oquab et al. 2024] as a conditioning signal injected into the cross-attention layers.

4.3 Stage 2: Part Structure Conditioned Generation and Articulation Prediction

4.3.1 Structure Condition Object Generation. Given the part-level structure decomposition from Stage 1, we obtain a set of part-wise *sparse voxels* that capture the coarse geometry and segmentation of the object. These sparse representations provide structural priors but lack fine-grained geometric details and appearance. In this stage, we synthesize detailed **geometry** and **appearance** for each part conditioned on the predicted coarse structure. Our design is related to OmniPart [Yang et al. 2025], which synthesizes parts conditioned on axis-aligned bounding boxes (AABBs) predicted by a separate box-prediction module. In contrast, we directly condition on the part-wise sparse voxels predicted in Stage 1, without relying on an additional bounding-box predictor.

Specifically, following TRELLIS and Omnipart, we tokenize sparse structured latents by flattening them into a 1D token sequence and injecting spatial information via positional encodings. Since Stage 1

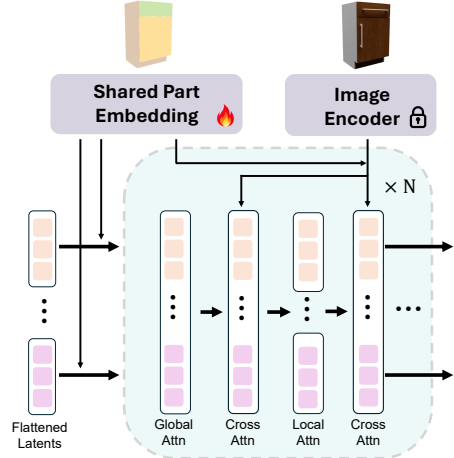


Fig. 3. Architecture of the Stage 1 model. To accommodate multi-part inputs, a subset of attention layers in the original TRELLIS network is repurposed to perform within-part local attention. With this modification, the model is fine-tuned on the target dataset.

provides accurate part-wise sparse structures, we concatenate tokens from all parts into a *global object token sequence* for object-level denoising (Fig. 4). To preserve part identity within this unified sequence, we introduce a learnable *part embedding* (separate from the part identity embedding used in Stage 1) and add it to every token belonging to the corresponding part, which allows the model to distinguish parts while reasoning globally over the entire object. Finally, the frozen sparse-latent decoder D_{SLAT} from TRELLIS reconstructs the per-part 3D representations and outputs the part geometries $\{\mathcal{G}_i\}_{i=1}^K$.

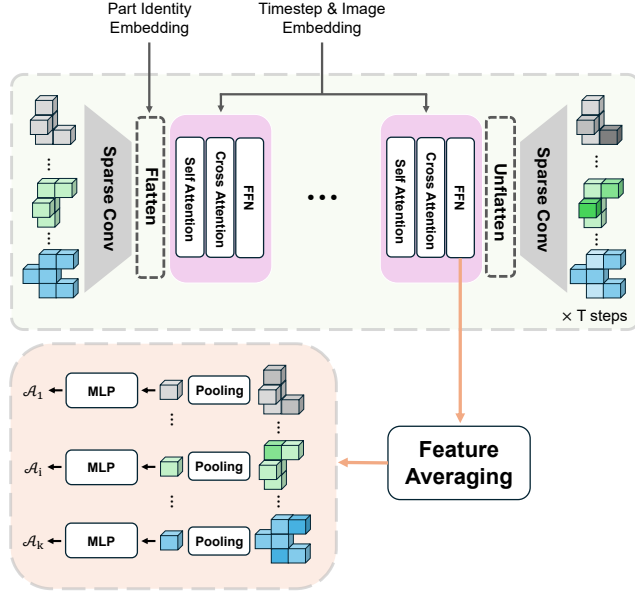


Fig. 4. Illustration of the Stage 2 pipeline. We cache a subset of intermediate features during part-token denoising. For each part, these features are averaged over selected inference timesteps and then pooled over the token dimension. A learned MLP then predicts the articulation parameters.

4.3.2 Articulation Regression.

Articulation Parameterization. Many datasets annotate fine-grained sub-components (e.g., handles or knobs) as separate nodes, even though they are attached to their parent parts via *fixed* joints and introduce no additional degrees of freedom. While prior methods [Liu et al. 2024a,b; Wu et al. 2025] model these sub-components in the articulation graph, we collapse all fixed-joint nodes into their parents and merge their geometry and appearance into the corresponding semantic part. This preserves the kinematic degrees of freedom while removing redundant nodes and edges. After this simplification, the resulting kinematic structure is shallow; accordingly, we adopt a semantics-driven parameterization where each part is assigned a semantic label (e.g., base, door, drawer), treat base as the root, and connect all other semantic parts directly to it.

Furthermore, following the experimental setting in prior work [Liu et al. 2024a; Wu et al. 2025], we consider objects that can be modeled by a depth-1 articulation tree (i.e., all movable parts are directly attached to a single fixed root), which covers many articulated objects in domestic environments. Under the depth-1 setting, once the base part is identified, we can set q_i deterministically for all non-root parts and define their articulation parameters relative to this part.

Predicting Joint Parameters from Part Tokens. The denoising backbone of our second stage operates on part-centric structured latents. After flattening, each part i is represented as a token sequence $\mathcal{Z}_i \in \mathbb{R}^{L_i \times D}$, where L_i (which may vary across parts) denotes the number of tokens for part i , and D is the token embedding dimension. Let $\mathbf{H}_i^t \in \mathbb{R}^{L_i \times D}$ denote the token features of part i from the *last* transformer block at diffusion step t .

Multi-step feature aggregation. Inspired by Diffusion Hyperfeatures [Luo et al. 2023], we aggregate denoiser features from multiple denoising steps, as features extracted at different diffusion timesteps capture complementary semantic information (Fig. 4). Given a set of selected steps \mathcal{T} , we first fuse part-level token features by averaging across timesteps:

$$\bar{\mathbf{H}}_i = \frac{1}{|\mathcal{T}|} \sum_{t \in \mathcal{T}} \mathbf{H}_i^t \in \mathbb{R}^{L_i \times D}. \quad (7)$$

We then summarize the fused tokens using mean and max pooling:

$$\bar{\mathbf{h}}_i = \left[\text{MeanPool}(\bar{\mathbf{H}}_i) \parallel \text{MaxPool}(\bar{\mathbf{H}}_i) \right] \in \mathbb{R}^{2D}, \quad (8)$$

where pooling is performed over the tokens of part i . The resulting feature is passed to an MLP g_ϕ to predict the articulation parameters:

$$\hat{\mathcal{A}}_i = \{\hat{t}_i, \hat{s}_i, \hat{o}_i, \hat{u}_i, \hat{p}_i\} = g_\phi(\bar{\mathbf{h}}_i). \quad (9)$$

This aggregation uses features from the denoising trajectory itself and adds negligible overhead. In practice, we set \mathcal{T} to the last S denoising steps, i.e., $\mathcal{T} = T - S + 1, \dots, T$, where T is the total number of diffusion steps.

4.4 Training

We train the flow model in Stage 1 using the same flow-matching formulation as TRELLIS [Xiang et al. 2024]. Specifically, we compute the flow-matching loss \mathcal{L}_{fm} in the part-latent space to optimize the denoising backbone.

For Stage 2, we jointly optimize the flow-matching objective and an articulation regression loss:

$$\mathcal{L} = \mathcal{L}_{\text{fm}} + \lambda \mathcal{L}_{\text{art}}.$$

We regress joint articulation parameters from intermediate part-token activations (Sec. 4.3.2) and supervise them with an ℓ_2 loss:

$$\mathcal{L}_{\text{art}} = \sum_{i=1}^K \left\| \hat{\mathcal{A}}_i - \mathcal{A}_i \right\|_2^2, \quad (10)$$

where \mathcal{A}_i and $\hat{\mathcal{A}}_i$ denote the ground-truth and predicted articulation parameter vectors for part i , respectively. Since flow matching training samples a single timestep per iteration, \mathcal{L}_{art} is computed using the corresponding (non-averaged) features at that timestep, rather than multi-step aggregated features.

5 Experiments

5.1 Implementation Details and Evaluation Setup.

Implementation Details. Our Part-Aware Flow Model is initialized from the Stage 1 checkpoint of TRELLIS, and the sparse transformer is initialized from the Stage 2 checkpoint of OmniPart [Yang et al. 2025]. We train the two stages separately. For both stages, we use a learning rate of 1×10^{-4} and train for 40K steps on 4 NVIDIA A800 GPUs with an effective batch size of 32. The articulation head g_ϕ is a six-layer MLP with hidden width 512. At inference time, we use CFG scale 7 for both stages and sample 25 denoising steps for Stage 1 and Stage 2. In the Part-Aware Flow Model, global and within-part local attention are interleaved across depth: even-indexed layers perform global attention, while odd-indexed layers apply within-part attention. For articulation prediction, we aggregate features from the last 20 denoising steps during inference. For part masks, we

consider two sources: (i) ground-truth annotations when available, and (ii) automatically generated masks obtained by a VLM-guided prompting pipeline followed by SAM2 [Ravi et al. 2024] refinement (VLM+SAM; see Appendix D for more details). Unless otherwise specified, we report results with both GT and VLM+SAM masks.

Dataset and Metrics. We follow prior works such as SINGAPO and DIPO [Wu et al. 2025] and use PartNet-Mobility [Xiang et al. 2020] for training. For evaluation, we report results on both PartNet-Mobility and ACD [Iliash et al. 2024], using the standard train/test splits from SINGAPO. Our test set contains 77 objects from PartNet-Mobility and 135 objects from ACD. For each object, we randomly sample two input images, resulting in 432 test inputs in total. To evaluate articulated object generation, we adopt four metrics commonly used in prior work: (1) $\text{dgIoU} \downarrow$, the generalized IoU between predicted and ground-truth part bounding boxes; (2) $\text{dcDist} \downarrow$, the Euclidean distance between predicted and ground-truth part centers; (3) $\text{dCD} \downarrow$, the Chamfer distance between predicted and ground-truth meshes; and (4) $\text{AOR} \uparrow$, the Average Overlapping Ratio measuring unrealistic inter-part collisions. We compute all metrics in both the resting state and articulated states, and report them separately using the prefixes **RS-** and **AS-**, respectively. Beyond geometric fidelity and articulation accuracy, we also evaluate *visual* consistency with the input image, *i.e.*, whether the generated object matches the specific instance in the observation. Following FreeArt3D [Chen et al. 2025a], we report an image-based similarity score using CLIP [Radford et al. 2021]. Specifically, we render the generated and ground-truth textured meshes from five random viewpoints under six articulation states, and compute the CLIP similarity between each rendering and the corresponding input image.

Baselines. We compare our method with representative articulated object generation approaches, including SINGAPO [Liu et al. 2024a], Articulate-Anything [Le et al. 2025], PhysX-3D [Cao et al. 2025a], PhysXAnything [Cao et al. 2025b], and ArtFormer [Su et al. 2025] as our primary baselines. We first consider retrieval-based methods. SINGAPO is a single-image retrieval-based pipeline that first infers the part connectivity graph and abstract part attributes, and then retrieves part meshes from a predefined database to assemble the final articulated object [Liu et al. 2024a]. Articulate-Anything is a VLM-driven system that retrieves part meshes from an asset library, assembles them into links, and then predicts joint parameters to output articulated models [Le et al. 2025]. In contrast to retrieval-based methods, PhysX-3D and PhysXAnything target physics-grounded, simulation-ready asset generation, producing explicit geometry together with kinematic (and related physical) attributes for downstream simulation and embodied tasks [Cao et al. 2025a,b]. ArtFormer parameterizes an articulated object as a tokenized kinematic tree and uses a transformer to generate both geometry codes and kinematic relations, enabling controllable and diverse articulated object synthesis [Su et al. 2025]. We additionally include FreeArt3D [Chen et al. 2025a], an optimization-based method, as a baseline. FreeArt3D is training-free and follows a per-instance optimization paradigm: given a few images of the same object under different articulation states, it jointly optimizes geometry and articulation to match the observations [Chen et al. 2025a]. Unlike the single-image methods above, FreeArt3D requires multiple images of the object captured under different articulation states.

5.2 General Results

We present qualitative comparisons on PartNet-Mobility and ACD in Fig. 5, and quantitative results in Tab. 2 and Tab. 1, respectively. For qualitative evaluation, all methods are visualized as textured meshes using the same Blender-based rendering pipeline.

Qualitative Results. As shown in Fig. 5, our method produces high-quality geometry and texture with strong consistency to the input image. Compared to all baselines, our reconstructions exhibit finer geometric details, more accurate part shapes, and more plausible articulation configurations. In addition, the predicted joint parameters closely match the ground truth, resulting in realistic articulated motion. Retrieval-based methods such as SINGAPO and Articulate-Anything often fail to recover instance-specific geometry and appearance. SINGAPO performs part retrieval without explicitly conditioning on image appearance, leading to noticeable deviations from the ground truth (*e.g.*, the first row). Articulate-Anything relies heavily on vision-language model reasoning, which can result in semantic misclassification; for example, in the seventh row, a white cabinet is incorrectly identified as a “door,” causing downstream errors in structure and articulation prediction.

Comparison with Optimization-based Methods. We further compare against FreeArt3D, which reconstructs articulated objects from multiple images under different articulation states using an SDS-based optimization procedure. In Fig. 6, we visualize both the final textured meshes and the raw part geometries by rendering each part in a distinct color. FreeArt3D often produces noisy or distorted part geometries and inconsistent part boundaries, leading to fragmented or inaccurate decompositions. In contrast, our method yields cleaner part geometries and more coherent part segmentation, despite using only a single input image. This demonstrates the advantage of our generative formulation over optimization-based approaches, even when the latter have access to multiple articulated views.

Quantitative Results. Quantitatively, our method consistently outperforms all baselines across all evaluated metrics. By directly synthesizing 3D geometry rather than retrieving parts from a database, our model produces more instance-specific shapes, resulting in improved resting-state accuracy (*e.g.*, lower RS- $d_{CD} \downarrow$). We also achieve stronger performance under articulated-state metrics, indicating more accurate articulation estimation and more reliable part motion.

Notably, our performance remains comparable when conditioning on VLM-predicted masks instead of ground-truth masks, with only minor degradation. This suggests that our approach is robust to imperfect part annotations and suitable for real-world scenarios where ground-truth masks are unavailable. Finally, we outperform all competing methods on the CLIP-based metric, indicating superior visual consistency with the input image and better preservation of instance-level appearance.

We report the runtime of all methods in Tab. 5 in the Appendix.

5.3 Ablation Studies

In **PAct**, articulation parameters are predicted by a lightweight module that decodes denoiser features from the Sparse Transformer (Stage 2). This module aggregates features from multiple denoising steps and regresses articulation parameters from the fused representation. To assess the effectiveness of this design, we conduct

Table 1. Comparison with baselines on the ACD Dataset [Iliash et al. 2024].

Methods\Metric	RS- $d_{\text{gloU}} \downarrow$	AS- $d_{\text{gloU}} \downarrow$	RS- $d_{\text{cDist}} \downarrow$	AS- $d_{\text{cDist}} \downarrow$	RS- $d_{\text{CD}} \downarrow$	AS- $d_{\text{CD}} \downarrow$	AOR \downarrow	CLIP \uparrow
SINGAPO [Liu et al. 2024a]	0.7272	0.7306	0.1585	0.1944	0.0090	0.0256	0.0115	0.8376
ArtFormer [Su et al. 2025]	1.3489	1.3876	0.3456	0.4414	0.0396	0.0825	0.0147	0.7690
PhysX3D [Cao et al. 2025a]	0.6449	0.6464	0.2591	0.3396	0.0209	0.0677	0.0960	0.8132
PhysXAnything [Cao et al. 2025b]	1.1673	1.1709	0.2965	0.3950	0.0162	0.0481	0.0099	0.8456
Arti-Anything [Le et al. 2025]	1.2677	1.2693	0.5632	0.5781	0.2583	0.2803	0.1236	0.8648
Ours + SAM+VLM Mask	0.5316	0.5412	0.1249	0.1656	0.0065	0.0218	0.0248	0.8901
Ours (GT Mask)	0.4182	0.4289	0.0830	0.1142	0.0060	0.0194	0.0107	0.8862

Table 2. Comparison with baselines on the PartNet-Mobility Dataset [Xiang et al. 2020].

Methods\Metric	RS- $d_{\text{gloU}} \downarrow$	AS- $d_{\text{gloU}} \downarrow$	RS- $d_{\text{cDist}} \downarrow$	AS- $d_{\text{cDist}} \downarrow$	RS- $d_{\text{CD}} \downarrow$	AS- $d_{\text{CD}} \downarrow$	AOR \downarrow	CLIP \uparrow
SINGAPO [Liu et al. 2024a]	0.5119	0.5166	0.1177	0.1505	0.0040	0.0202	0.0097	0.8779
ArtFormer [Su et al. 2025]	1.3165	1.3212	0.3542	0.5099	0.0504	0.1849	0.0191	0.7877
PhysX3D [Cao et al. 2025a]	0.7610	0.7637	0.3233	0.4562	0.0115	0.1204	0.2125	0.7972
PhysXAnything [Cao et al. 2025b]	0.9596	0.9661	0.2538	0.4034	0.0097	0.1106	0.0056	0.8859
Arti-Anything [Le et al. 2025]	0.6865	0.6969	0.1386	0.3414	0.0107	0.1230	0.0056	0.8795
Ours + SAM+VLM Mask	0.2485	0.2736	0.0707	0.1191	0.0019	0.0176	0.0233	0.8996
Ours (GT Mask)	0.1395	0.1395	0.0202	0.0653	0.0016	0.0139	0.0011	0.9053

ablation studies on PartNet-Mobility along three axes: (1) the number of denoising steps used for feature aggregation; (2) predicting articulation from Stage 2 features versus Stage 1 (Part-Aware Flow Model) features; and (3) replacing the deterministic regression head with a generative, flow-matching-based articulation predictor.

Number of Denoising Steps. As shown in Tab. 3 (in the Appendix), aggregating features from multiple denoising steps consistently improves articulation prediction. We evaluate step counts $S = \{1, 15, 20\}$. Using a single step provides limited context and leads to unstable predictions, while aggregating more steps improves performance with diminishing returns. Overall, aggregating features from 20 denoising steps yields the best results and is used as the default setting.

Stage 1 vs. Stage 2 Features. Predicting articulation from Stage 1 features (“Stage 1-Articulation”) performs significantly worse than using Stage 2 features. This reflects the difference in representation: Stage 1 features primarily encode coarse structural information, whereas Stage 2 features are more informative and globally contextualized through object-level denoising, making them better suited for articulation estimation.

Regression vs. Generative Articulation prediction. Replacing the deterministic MLP regression head with a flow-matching-based generative predictor (“FM Articulation”) does not yield consistent improvements on PartNet-Mobility, while introducing additional training and inference complexity. We therefore adopt the simpler regression-based articulation module in all experiments.

5.4 Real-World Articulated Object Generation

Beyond standard benchmarks, we collect a small set of real-world images containing commonly seen articulated objects (e.g., cabinets, desks, and microwaves) and evaluate our method under the same

single-image setting. As shown in Fig. 7, our approach generalizes well to these in-the-wild inputs, producing articulated reconstructions with coherent part decomposition, plausible geometry, and visually consistent textures. Despite the domain gap between curated dataset renderings and real photographs, our method remains robust to variations in lighting and appearance, yielding stable part-level generation and reasonable articulation prediction. These results suggest that the learned part-centric priors transfer beyond the training distribution.

5.5 Mask-Controlled Generation

A single input image may admit multiple valid part decompositions, leading to different but plausible articulation structures. To enable controllable generation under such ambiguity, we use a semantic part mask as an explicit conditioning signal. By specifying the set of semantic parts, the mask directly determines the target decomposition and the resulting articulated object. Fig. 8 illustrates this effect using two alternative masks per image. For example, in the first row, different masks guide the model to generate either (i) two doors only or (ii) two doors with two drawers, while preserving consistent appearance and plausible joint configurations. This mask-based conditioning enables controllable generation and reduces ambiguity in part structure and articulation for real-world images.

6 Limitations and Conclusion

Scaling to many-part objects. Our method currently struggles to scale to articulated objects with a large number of parts. This reflects both model capacity/optimization challenges and dataset bias: in commonly used benchmarks, hinge-based objects with more than eight parts are rare, limiting supervision for complex multi-part configurations. Addressing this limitation likely requires improved modeling as well as broader training data coverage.

Unseen or occluded parts. We assume that all relevant parts are visible in the input image. When functional components are occluded or only appear under certain articulation states (e.g., a drawer behind a closed cabinet door), the model may fail to infer and generate them. Incorporating occlusion reasoning and stronger priors for completing unseen components is a promising direction. **Beyond shallow tree structures.** We adopt a simplified kinematic formulation that is effective for many common categories with shallow, tree-structured articulation. Extending to objects with richer kinematic dependencies (e.g., shared constraints or closed-chain mechanisms) may require explicit graph-based constraints. Developing scalable and learnable formulations for such settings remains an important direction for future work.

Conclusion. We present a part-centric framework for single-image articulated object generation. Our method decomposes an object into semantic parts and predicts their articulations, enabling faithful reconstruction of both geometry and motion for common hinge-based objects. Extensive experiments show that our approach improves articulation accuracy while maintaining high-quality part geometry, and remains competitive against strong baselines on standard benchmarks.

References

Ziang Cao, Zhaoxi Chen, Liang Pan, and Ziwei Liu. 2025a. PhysX-3D: Physical-Grounded 3D Asset Generation. *arXiv preprint arXiv:2507.12465* (2025).

Ziang Cao, Fangzhou Hong, Zhaoxi Chen, Liang Pan, and Ziwei Liu. 2025b. PhysX-Anything: Simulation-Ready Physical 3D Assets from Single Image. *arXiv preprint arXiv:2511.13648* (2025).

Chuhao Chen, Isabella Liu, Xinyue Wei, Hao Su, and Minghua Liu. 2025a. FreeArt3D: Training-Free Articulated Object Generation using 3D Diffusion. In *SIGGRAPH Asia 2025 Conference Papers*.

Minghao Chen, Roman Shapovalov, Iro Laina, Tom Monnier, Jianyuan Wang, David Novotny, and Andrea Vedaldi. 2024. PartGen: Part-level 3D Generation and Reconstruction with Multi-View Diffusion Models. *arXiv preprint arXiv:2412.18608* (2024).

Minghao Chen, Jianyuan Wang, Roman Shapovalov, Tom Monnier, Hyunyoung Jung, Dilin Wang, Rakesh Ranjan, Iro Laina, and Andrea Vedaldi. 2025b. AutoPartGen: Autoregressive 3D Part Generation and Discovery. *arXiv preprint arXiv:2507.13346* (2025).

Daoyi Gao, Yawar Siddiqui, Lei Li, and Angela Dai. 2024. MeshArt: Generating Articulated Meshes with Structure-guided Transformers. *arXiv preprint arXiv:2412.11596* (2024).

Yumeng He, Ying Jiang, Jiayin Lu, Yin Yang, and Chenfanfu Jiang. 2025. SPARK: Sim-ready Part-level Articulated Reconstruction with VLM Knowledge. *arXiv preprint 2512.01629* (2025).

Yicong Hong, Kai Zhang, Jiaxiang Gu, Sai Bi, Yang Zhou, Difan Liu, Feng Liu, Kalyan Sunkavalli, Trung Bui, and Hao Tan. 2023. Lrm: Large reconstruction model for single image to 3d. *arXiv preprint arXiv:2311.04400* (2023).

Cheng-Chun Hsu, Zhenyu Jiang, and Yuke Zhu. 2023. Ditto in the house: Building articulation models of indoor scenes through interactive perception. In *ICRA*.

Denys Iliash, Hanxiao Jiang, Yiming Zhang, Manolis Savva, and Angel X Chang. 2024. S2O: Static to openable enhancement for articulated 3D objects. *arXiv preprint arXiv:2409.18896* (2024).

Zhenyu Jiang, Cheng-Chun Hsu, and Yuke Zhu. 2022. Ditto: Building digital twins of articulated objects from interaction.

Bernhard Kerbl, Georgios Kopanas, Thomas Leimkühler, and George Drettakis. 2023. 3D Gaussian Splatting for Real-Time Radiance Field Rendering. *ACM Transactions on Graphics* 42, 4 (July 2023).

Long Le, Jason Xie, William Liang, Hung-Ju Wang, Yue Yang, Yecheng Jason Ma, Kyle Vedder, Arjun Krishna, Dinesh Jayaraman, and Eric Eaton. 2025. Articulate-anything: Automatic modeling of articulated objects via a vision-language foundation model. *ICLR* (2025).

Jiahui Lei, Congyue Deng, William B Shen, Leonidas J Guibas, and Kostas Daniilidis. 2023. Nap: Neural 3d articulated object prior. *Advances in Neural Information Processing Systems* (2023).

Zizhang Li, Cheng Zhang, Zhengqin Li, Henry Howard-Jenkins, Zhaoyang Lv, Chen Geng, Jiajun Wu, Richard Newcombe, Jakob Engel, and Zhao Dong. 2025. ART: Articulated Reconstruction Transformer. *arXiv preprint arXiv:2512.14671* (2025).

Xinyu Lian, Zichao Yu, Ruiming Liang, Yitong Wang, Li Ray Luo, Kaixu Chen, Yuanzhen Zhou, Qihong Tang, Xudong Xu, Zhaoyang Lyu, et al. 2025. Infinite Mobility: Scalable High-Fidelity Synthesis of Articulated Objects via Procedural Generation. *arXiv preprint arXiv:2503.13424* (2025).

Shengjie Lin, Jiading Fang, Muhammad Zubair Irshad, Vitor Campagnolo Guizilini, Rares Andrei Ambrus, Greg Shakhnarovich, and Matthew R Walter. 2025a. SplArt: Articulation Estimation and Part-Level Reconstruction with 3D Gaussian Splatting. *arXiv preprint arXiv:2506.03594* (2025).

Yuchen Lin, Chenguo Lin, Panwang Pan, Honglei Yan, Yiqiang Feng, Yadong Mu, and Katerina Fragkiadaki. 2025b. PartCrafter: Structured 3D Mesh Generation via Compositional Latent Diffusion Transformers. *arXiv preprint arXiv:2506.05573* (2025).

Jiayi Liu, Denys Iliash, Angel X Chang, Manolis Savva, and Ali Mahdavi-Amiri. 2024a. SINGAPO: Single Image Controlled Generation of Articulated Parts in Object. *arXiv preprint arXiv:2410.16499* (2024).

Jiayi Liu, Ali Mahdavi-Amiri, and Manolis Savva. 2023. PARIS: Part-level Reconstruction and Motion Analysis for Articulated Objects. In *ICCV*.

Jiayi Liu, Hou In Ivan Tam, Ali Mahdavi-Amiri, and Manolis Savva. 2024b. CAGE: Controllable Articulation GEneration. *CVPR* (2024).

Yu Liu, Baoxiong Jia, Ruijie Lu, Chuyue Gan, Huayu Chen, Junfeng Ni, Song-Chun Zhu, and Siyuan Huang. 2025a. VideoArtGS: Building Digital Twins of Articulated Objects from Monocular Video. *arXiv preprint arXiv:2509.17647* (2025).

Yu Liu, Baoxiong Jia, Ruijie Lu, Junfeng Ni, Song-Chun Zhu, and Siyuan Huang. 2025b. Building Interactable Replicas of Complex Articulated Objects via Gaussian Splatting. In *The Thirteenth International Conference on Learning Representations*.

Grace Luo, Lisa Dunlap, Dong Huk Park, Aleksander Holynski, and Trevor Darrell. 2023. Diffusion Hyperfeatures: Searching Through Time and Space for Semantic Correspondence. *Advances in Neural Information Processing Systems* (2023).

Changfeng Ma, Yang Li, Xinhao Yan, Jiachen Xu, Yunhan Yang, Chunshi Wang, Zibo Zhao, Yanwen Guo, Zhuo Chen, and Chunhao Guo. 2025. P3-sam: Native 3d part

segmentation. *arXiv preprint arXiv:2509.06784* (2025).

Zhao Mandi, Yijia Weng, Dominik Bauer, and Shuran Song. 2024. Real2Code: Reconstruct Articulated Objects via Code Generation. *arXiv preprint arXiv:2406.08474* (2024).

Yongsen Mao, Yiming Zhang, Hanxiao Jiang, Angel X Chang, and Manolis Savva. 2022. MultiScan: Scalable RGBD scanning for 3D environments with articulated objects. *CVPR* (2022).

Neil Nie, Samir Yitzhak Gadre, Kiana Ehsani, and Shuran Song. 2022. Structure from action: Learning interactions for articulated object 3d structure discovery. *arXiv preprint arXiv:2207.08997* (2022).

Maxime Oquab, Timothée Darzet, Théo Moutakanni, Huy V. Vo, Marc Szafraniec, Vasil Khalidov, Pierre Fernandez, Daniel HAZIZA, Francisco Massa, Alaaeldin El-Nouby, Mido Assran, Nicolas Ballas, Wojciech Galuba, Russell Howes, Po-Yao Huang, Shang-Wen Li, Ishan Misra, Michael Rabbat, Vasu Sharma, Gabriel Synnaeve, Xu Hu, Herve Jegou, Julien Mairal, Patrick Labatut, Armand Joulin, and Piotr Bojanowski. 2024. DINOv2: Learning Robust Visual Features without Supervision. *Transactions on Machine Learning Research* (2024).

Xiaowen Qiu, Jincheng Yang, Yian Wang, Zhehuan Chen, Yufei Wang, Tsun-Hsuan Wang, Zhou Xian, and Chuang Gan. 2025. Articulate AnyMesh: Open-Vocabulary 3D Articulated Objects Modeling. *arXiv preprint arXiv:2502.02590* (2025).

Alec Radford, Jong Wook Kim, Chris Hallacy, Aditya Ramesh, Gabriel Goh, Sandhini Agarwal, Girish Sastry, Amanda Askell, Pamela Mishkin, Jack Clark, et al. 2021. Learning transferable visual models from natural language supervision. In *International conference on machine learning*. PMLR, 8748–8763.

Nikhila Ravi, Valentin Gabeur, Yuan-Ting Hu, Ronghang Hu, Chaitanya Ryali, Tengyu Ma, Haitham Khedr, Roman Rädle, Chloe Rolland, Laura Gustafson, Eric Mintun, Junting Pan, Kalyan Vasudev Alwala, Nicolas Carion, Chao-Yuan Wu, Ross Girshick, Piotr Dollár, and Christoph Feichtenhofer. 2024. SAM 2: Segment Anything in Images and Videos. *arXiv preprint arXiv:2408.00714* (2024).

ByteDance Seed3D Team. 2025. Seed3D 1.0: From Images to High-Fidelity Simulation-Ready 3D Assets. *Technique Report* (2025).

Chaoyue Song, Jiacheng Wei, Chuan Sheng Foo, Guosheng Lin, and Faya Liu. 2024. REACTO: Reconstructing Articulated Objects from a Single Video.

Jiayi Su, Youhe Feng, Zheng Li, Jinhua Song, Yangfan He, Botao Ren, and Botian Xu. 2025. ArtFormer: Controllable Generation of Diverse 3D Articulated Objects. In *Proceedings of the IEEE/CVF Conference on Computer Vision and Pattern Recognition (CVPR)*. 1894–1904.

Stanislaw Szemanowicz, Christian Rupprecht, and Andrei Vedaldi. 2024. Splatter image: Ultra-fast single-view 3d reconstruction. In *Proceedings of the IEEE/CVF Conference on Computer Vision and Pattern Recognition (CVPR)*. 10208–10217.

Jiaxiang Tang, Zhaoxi Chen, Xiaokang Chen, Tengfei Wang, Gang Zeng, and Ziwei Liu. 2024. Lgn: Large multi-view gaussian model for high-resolution 3d content creation. In *European Conference on Computer Vision*. Springer, 1–18.

Jiaxiang Tang, Ruiji Lu, Zhaoshuo Li, Zekun Hao, Xuan Li, Fangyin Wei, Shuran Song, Gang Zeng, Ming-Yu Liu, and Tsung-Yi Lin. 2025. Efficient Part-level 3D Object Generation via Dual Volume Packing. *arXiv preprint arXiv:2506.09980* (2025).

Tencent Hunyuan3D Team. 2024. Hunyuan3D 1.0: A Unified Framework for Text-to-3D and Image-to-3D Generation. *arXiv preprint arXiv:2411.02293* (2024).

Tencent Hunyuan3D Team. 2025a. Hunyuan3D 2.0: Scaling Diffusion Models for High Resolution Textured 3D Assets Generation. *arXiv preprint arXiv:2501.12202* (2025).

Tencent Hunyuan3D Team. 2025b. Hunyuan3D 2.5: Towards High-Fidelity 3D Assets Generation with Ultimate Details. *arXiv preprint arXiv:2506.16504* (2025).

Dmitry Tochilkin, David Pankratz, Zexiang Liu, Zixuan Huang, Adam Letts, Yangguang Li, Ding Liang, Christian Laforte, Varun Jampani, and Yan-Pei Cao. 2024. TripoSR: Fast 3D Object Reconstruction from a Single Image. *arXiv preprint arXiv:2403.02151* (2024).

Jiawei Wang, Dingyou Wang, Jiaming Hu, Qixuan Zhang, Jingyi Yu, and Lan Xu. 2025. Kinemafy: Open-Vocabulary Synthesis of High-DoF Articulated Objects. *arXiv preprint arXiv:2511.01294* (2025).

Peng Wang, Hao Tan, Sai Bi, Yinghao Xu, Fujun Luan, Kalyan Sunkavalli, Wenping Wang, Zexiang Xu, and Kai Zhang. 2024. PF-LRM: Pose-Free Large Reconstruction Model for Joint Pose and Shape Prediction. (2024). <https://openreview.net/forum?id=noe76eRcPC>

Ruqi Wu, Xinjie Wang, Liu Liu, Chunle Guo, Jiaxiong Qiu, Chongyi Li, Lichao Huang, Zhizhong Su, and Ming-Ming Cheng. 2025. DIPO: Dual-State Images Controlled Articulated Object Generation Powered by Diverse Data. *Advances in Neural Information Processing Systems* 39 (2025).

Fanbo Xiang, Yuzhe Qin, Kaichun Mo, Yikuan Xia, Hao Zhu, Fangchen Liu, Minghua Liu, Hanxiao Jiang, Yifu Yuan, He Wang, et al. 2020. Sapien: A simulated part-based interactive environment. *CVPR* (2020).

Jianfeng Xiang, Xiaoxue Chen, Sicheng Xu, Ruicheng Wang, Zelong Lv, Yu Deng, Hongyuan Zhu, Yue Dong, Hao Zhao, Nicholas Jing Yuan, and Jiaolong Yang. 2025. Native and Compact Structured Latents for 3D Generation. *arXiv preprint arXiv:2512.14692* (2025).

Jianfeng Xiang, Zelong Lv, Sicheng Xu, Yu Deng, Ruicheng Wang, Bowen Zhang, Dong Chen, Xin Tong, and Jiaolong Yang. 2024. Structured 3D Latents for Scalable and Versatile 3D Generation. *arXiv preprint arXiv:2412.01506* (2024).

Xinhao Yan, Jiachen Xu, Yang Li, Changfeng Ma, Yunhan Yang, Chunshi Wang, Zibo Zhao, Zeqiang Lai, Yunfei Zhao, Zhuo Chen, et al. 2025. X-Part: high fidelity and structure coherent shape decomposition. *arXiv preprint arXiv:2509.08643* (2025).

Yunhan Yang, Yufan Zhou, Yuan-Chen Guo, Zi-Xin Zou, Yukun Huang, Ying-Tian Liu, Hao Xu, Ding Liang, Yan-Pei Cao, and Xihui Liu. 2025. Omnipart: Part-aware 3d generation with semantic decoupling and structural cohesion. *arXiv preprint arXiv:2507.06165* (2025).

Sylvia Yuan, Ruoxi Shi, Xinyue Wei, Xiaoshuai Zhang, Hao Su, and Minghua Liu. 2025. LARM: A Large Articulated-Object Reconstruction Model. *arXiv preprint arXiv:2511.11563* (2025).

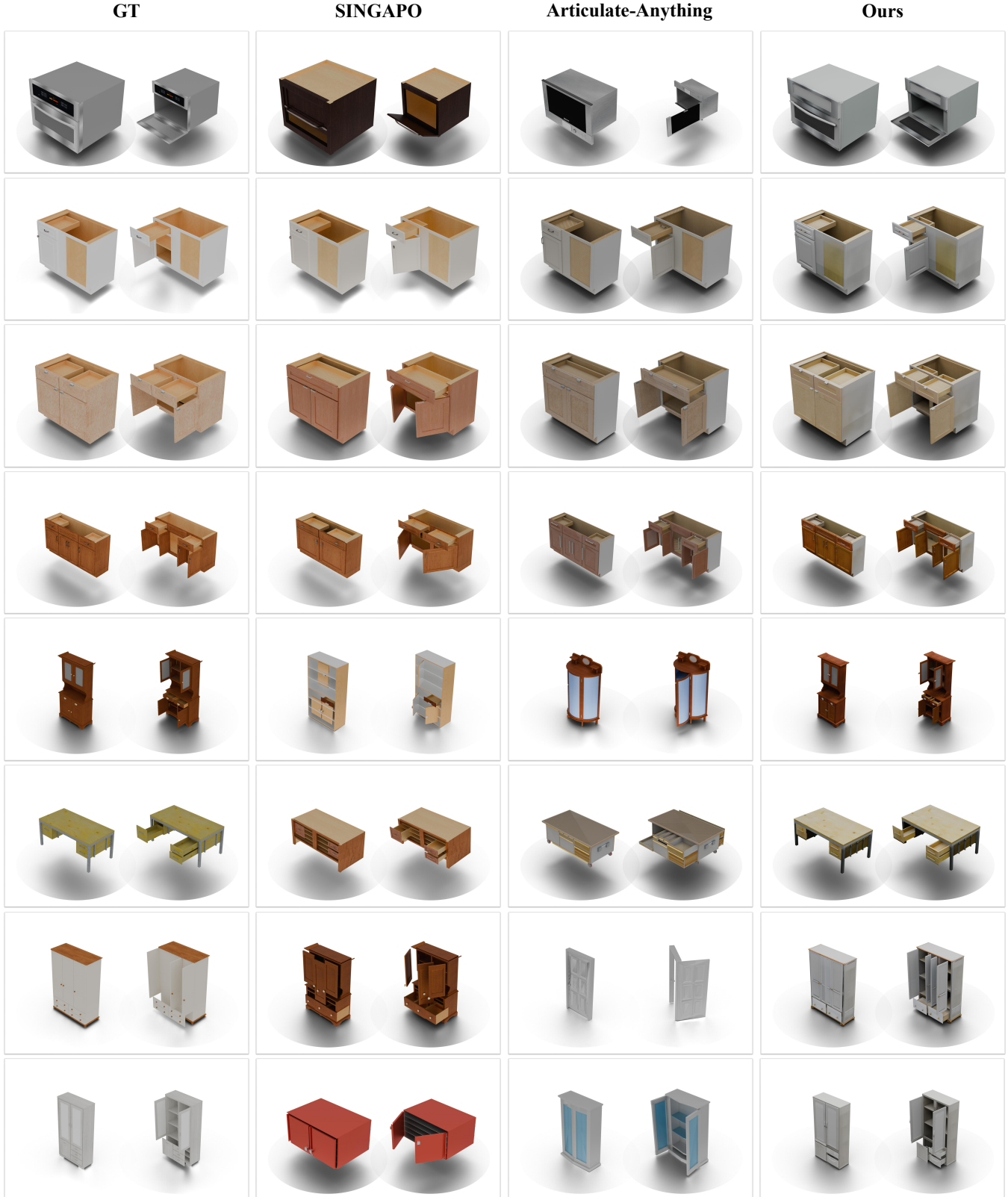


Fig. 5. Qualitative comparison on the PartNet-Mobility [Xiang et al. 2020] and ACD [Iliash et al. 2024] datasets. We compare **PAct** with SINGAPO [Liu et al. 2024a], Articulate-Anything [Le et al. 2025].



Fig. 6. Qualitative comparison with FreeArt3D [Chen et al. 2025a]. We visualize the geometry of different parts using distinct colors.

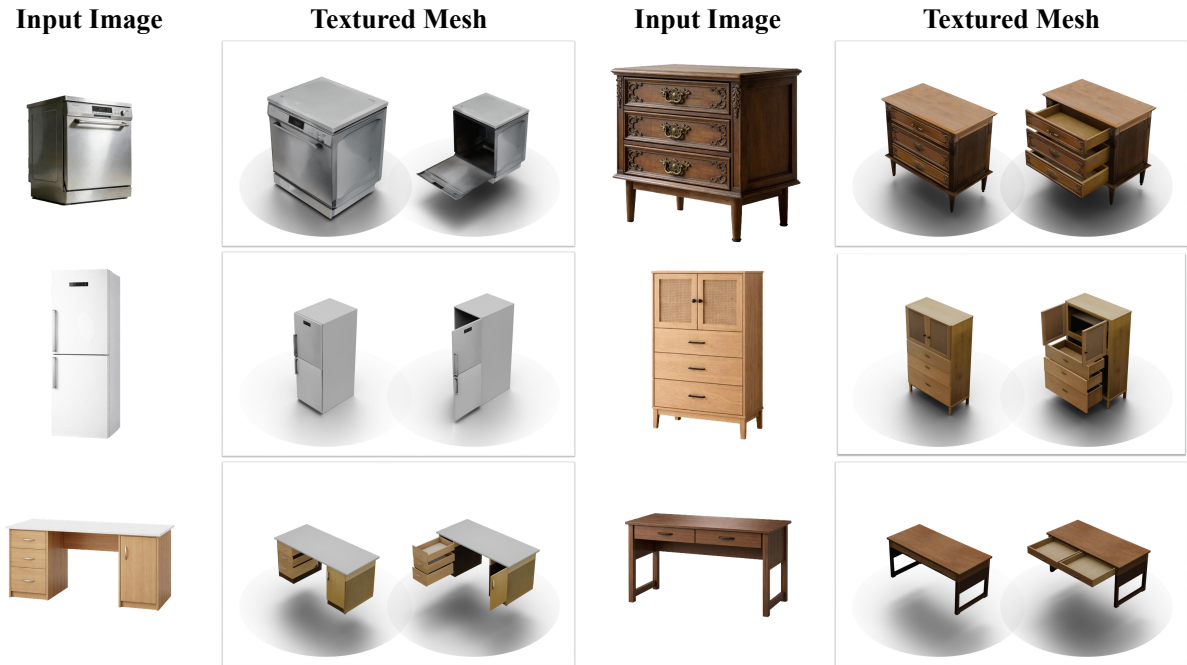


Fig. 7. Qualitative results on the in-the-wild images collected from the internet.

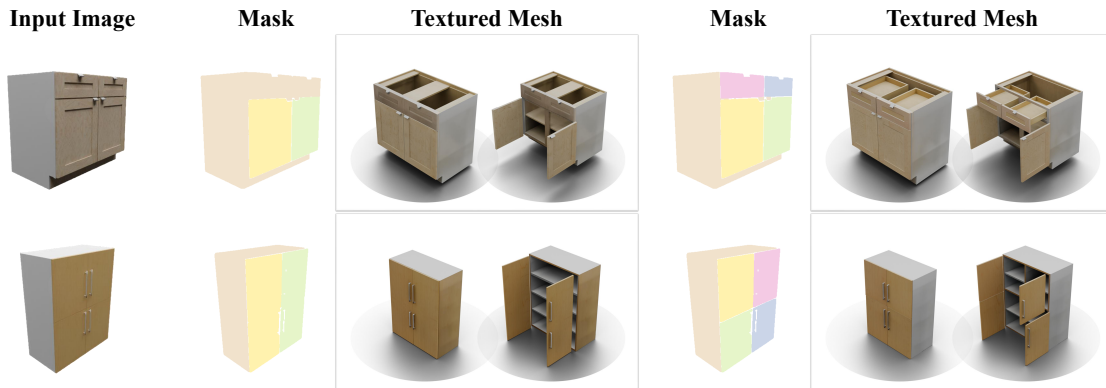


Fig. 8. Qualitative results using the same images but with different masks as control signals.

A Additional Implementation Details

For SINGAPO [Liu et al. 2024a], a retrieval-based method, we use the official codebase to retrieve parts from its preprocessed datasets and provide the corresponding ground-truth articulation graphs as input. For ArtFormer [Su et al. 2025], PhysX-3D [Cao et al. 2025a], and PhysXAnything [Cao et al. 2025b], we conduct experiments using their official code and released checkpoints with their default inference settings unless stated otherwise. For FreeArt3D [Chen et al. 2025a], we use the generated results released by the authors for comparison. Regarding Articulate-Anything [Le et al. 2025], the official implementation depends on the deprecated Gemini-1.5-Flash API; therefore, we replace it with Gemini-2.5-Flash (a newer available endpoint) while keeping the original prompts and other steps unchanged. Below, we provide additional details on (i) the ArtFormer image-to-text surrogate setting, (ii) the CLIP-based similarity evaluation, and (iii) the PhysX-3D part-level articulation extraction used to match our evaluation protocol.

ArtFormer Image-to-text Surrogate Setting. Since our benchmark provides images as inputs, we evaluate baselines under an image-conditioned setting when possible. However, ArtFormer does not release an image-conditioned model and does not provide the full training code to reproduce such a setting end-to-end. To enable a comparable image-based evaluation while staying faithful to their released *text-based* model, we follow their preprocessing procedure to first generate an image description (caption) for each input image, converting the image condition into a textual prompt (*image* \rightarrow *caption*). We then feed this text prompt into the official *text-to-3D* generation pipeline. In other words, ArtFormer is evaluated through an “*image* \rightarrow *caption* \rightarrow *text-to-3D*” surrogate pipeline that directly leverages its released text model.

CLIP-based Similarity Evaluation. For CLIP evaluation, we follow the protocol of FreeArt3D [Chen et al. 2025a]. For each object, we sample 6 articulation states, and for each state we render 5 viewpoints. For each viewpoint, we render both the generated mesh and the corresponding ground-truth mesh under the same camera and compute CLIP *image-image* similarity using CLIP *ViT-L/14@336px*. We then average the similarities over all states and viewpoints to obtain a semantic similarity score per object. Since ArtFormer does not generate textures, we evaluate ArtFormer using renders of the *untextured (white/gray) mesh* for both its outputs and the corresponding ground-truth objects, to avoid bias due to missing textures; for all other methods we use textured renders.

PhysX-3D Articulation Extraction. PhysX-3D outputs a holistic object (e.g., a mesh) with per-vertex kinematic predictions, rather than explicit *part-level* geometry and kinematic parameters. Therefore, we convert its per-vertex outputs into a part-level articulated representation to match our evaluation protocol. Specifically, we cluster vertices with the same predicted *Part ID* to decompose the holistic shape into rigid parts. Meanwhile, we build the kinematic tree by assigning each part a *Parent ID* via majority voting over its vertices, which improves robustness to boundary noise and defines the parent-child relations between parts. For joint parameters, we aggregate per-vertex predictions within each part: the joint type is determined by majority vote, while continuous attributes (axis

direction, pivot point, and motion range) are averaged, with the axis direction re-normalized to obtain consistent kinematic parameters for each part.

B Post-processing on Predicted Articulation.

To obtain a more physically plausible placement of the *revolute* joint axis, we apply a simple post-processing step to the predicted *axis origin*. Specifically, for each revolute joint, we project the regressed axis origin onto the part’s axis-aligned bounding box (AABB) by replacing it with the closest point on the AABB *surface*. The projected origin is then used for subsequent articulation evaluation.

C Supplementary Comparison

In Table 4, we compare baseline methods and summarize their key capabilities. *Geometry* indicates whether the method generates 3D shape outputs (e.g., meshes or point clouds); *Texture* indicates whether it synthesizes appearance; and *Part-level Articulation* indicates whether it outputs part-level articulation information. Beyond outputs, *Non-Retrieval* indicates whether the method operates without retrieving examples from a predefined database at inference time. We additionally report runtime performance in Table 5 (end-to-end inference time per object under the same hardware setting).

D VLM-Guided Part Analysis and Mask Annotation

Articulated objects often admit multiple plausible part decompositions due to the presence of several movable components. To improve the controllability of articulated part generation, we incorporate an additional 2D part mask \mathcal{M} as a conditioning input, which explicitly specifies the desired part decomposition in the input image. To automate mask acquisition, we first use SAM2 [Ravi et al. 2024] to produce fine-grained segmentation masks. Since SAM2 may over-segment an articulated part into multiple fragments, we further employ a vision-language model (VLM, e.g., GPT-5) to identify masks that belong to the same part and merge them into a single part mask. This produces a cleaner, part-level decomposition that better matches the articulation structure and serves as our final conditioning mask \mathcal{M} . The entire pipeline is built upon the OmniPart [Yang et al. 2025] codebase and consists of the following stages.

Stage 0: Pre-Process. Prior to segmentation, we employ GPT-5 (specifically, version gpt-5-2025-08-07) to determine the granularity for part segmentation, utilizing the prompting strategy illustrated in Fig. 9.

Stage 1: Part Classification. In the classification phase, the Segment Anything Model (SAM) [Ravi et al. 2024] first generates candidate part segmentations with the granularity proposed in the pre-processing stage. The VLM is then prompted, as shown in Fig. 10, to classify each segment as either articulated or fixed.

Stage 2: Part Merging. Building upon the labeled RGB images and part classifications obtained in Stage 1, the VLM performs a semantic merging process to consolidate segments that belong to the same articulated part. For example, SAM2 [Ravi et al. 2024] often treats a door and its handle as two distinct entities. In our setting, we require these components to be recognized as a single kinematic body.

Table 3. Ablation study with different configurations on the PartNet-Mobility dataset [Xiang et al. 2020].

Methods\Metric	RS- $d_{\text{gIoU}} \downarrow$	AS- $d_{\text{gIoU}} \downarrow$	RS- $d_{\text{cDist}} \downarrow$	AS- $d_{\text{cDist}} \downarrow$	RS- $d_{\text{CD}} \downarrow$	AS- $d_{\text{CD}} \downarrow$	AOR \downarrow	CLIP \uparrow
$S = 1$	0.1734	0.1999	0.0300	0.0966	0.0017	0.0220	0.0088	0.8903
$S = 15$	0.1737	0.2002	0.0320	0.0762	0.0018	0.0145	0.0090	0.8911
$S = 20$	0.1395	0.1395	0.0202	0.0653	0.0016	0.0139	0.0011	0.9053
Stage 1-Articulation	0.1615	0.1878	0.0302	0.0889	0.0016	0.0210	0.0068	0.8903
FM Articulation	0.3615	0.4132	0.1263	0.3019	0.0021	0.1100	0.0190	0.8803
Ours (GT Mask)	0.1395	0.1395	0.0202	0.0653	0.0016	0.0139	0.0011	0.9053

Table 4. Comparison of representative methods and their capabilities.

Methods	Geometry	Texture	Part-level Articulation	Non-Retrieval
SINGAPO [Liu et al. 2024a]	✓	✗	✓	✗
ArtFormer [Su et al. 2025]	✓	✗	✓	✓
PhysX-3D [Cao et al. 2025a]	✓	✓	✗	✓
Articulate-Anything [Le et al. 2025]	✗	✗	✓	✗
Ours	✓	✓	✓	✓

Table 5. Runtime comparison between our method and baseline methods.
All measurements were conducted on a single NVIDIA A800 GPU.

Ours	ArtiAny	ArtFormer	SINGAPO	PhysX3D	PhysXAnything	FreeArt3D
~15s	~3min	~155s	~8s	~96s	~20min	~10min

This merging process effectively corrects the over-segmentation artifacts produced by SAM2, yielding a coherent, articulation-aware segmentation that serves as our final conditioning input \mathcal{M} .

Stage 0 Prompt

You are given:
 1) An image of a real-world articulated object
 2) A prior analysis of its FUNCTIONAL and MECHANICAL structure (Stage 1)

Your task:
 Recommend an appropriate value for the parameter: Minimum Segment Size

CONSTRAINTS:
 - The value MUST be between 1000 and 2000 (inclusive).
 - The value MUST be an integer multiple of 200.
 - Valid values are: 1000, 1200, 1400, 1600, 1800, 2000.

Output format:
 Minimum Segment Size: <1000

Fig. 9. Prompt designed for GPT-5 during the pre-processing stage to determine appropriate segmentation granularity.

Stage 1 Prompt

You are given an image of a real-world object

Task:
 1. Briefly identify what the object appears to be.
 2. From a FUNCTIONAL and MECHANICAL perspective, estimate:
 - How many articulated (movable) parts the object has.
 - How many fixed (non-movable) parts the object has.

Output format:
 Object: <short description>
 Articulated parts: <number>
 Fixed parts: <number>

Fig. 10. Prompt designed for GPT-5 to perform part classification.

Stage 2 Prompt

You are given THREE images of the SAME object:

- 1) Original RGB image (real-world reference)
- 2) Pre-merge segmentation image with NUMERIC segmentation IDs overlaid
- 3) Pre-merge segmentation image showing the ORIGINAL object appearance

From Stage 1, you are told {stage1_result}

TASK DESCRIPTION:
 You are provided with three views of an object.
 Your goal is to merge segmentation IDs to identify the ARTICULATED parts (movable parts).
 You must merge aggressively to find the MINIMUM number of articulated parts.

GUIDELINES FOR MINIMIZING PARTS:

1. An 'articulated part' includes everything attached to it.
 - Example: A Door includes the panel, the handle, the glass window, and the hinges.
 These are ALL 1 part. Merge their IDs.
- Example: A Drawer includes the drawer face and the knob/handle. Merge them.
2. Do not separate handles from doors.
3. Do not count the fixed body/frame as an articulated part yet.

OUTPUT FORMAT:
 Please follow this format exactly:
 Step 1: Reasoning
 [Explain your thinking here. Which IDs make up the door? Which make up the drawer?
 Why are you merging them?
 Step 2: Final Output
 FINAL MERGE GROUPS: <group_1_IDs separated by commas>[;<group_2_IDs>;...]

EXAMPLES:
 Step 1: Reasoning
 IDs 3 and 4 are the handle and the door panel, they move together. ID 8 is a separate drawer.
 Step 2: Final Output
 FINAL MERGE GROUPS: 3,4;8

Fig. 11. Prompt for GPT-5 in the merging stage to generate articulated part mask.